# Influence of Transient Flight Maneuvers on Rotor Wake Dynamics and Noise Radiation


Christopher C. Hennes,[*] Hsuan-Nien Chen,[†] and Kenneth S.Brentner[‡]
The Pennsylvania State University
University Park, Pennsylvania
and
Shreyas Ananthan[§] and J. Gordon Leishman[¶]
The University of Maryland
College Park, Maryland



## Abstract

This paper presents a study of three flight maneuvers using a rotorcraft aeroacoustics model: "pop-up," "pop-down," and an arrested descent. A time-accurate free-vortex rotor wake model and a maneuvering rotor noise prediction code were used to compute the noise. All rotorcraft motions and rigid body blade motions were included in the respective models. The wake geometry and its development is described. It is shown that the magnitude and directivity of the noise is strongly dependent on the rotor wake characteristics when blade-vortex interactions occur. In the transient arrested descent maneuver, the wake geometry becomes extremely complicated, and a significant increase in both nonimpulsive and impulsive noise is predicted.


## Notation

| | |
|---|---|
| $c$ | Speed of sound (quiescent medium), ms$^{-1}$ |
| $C_l$ | Sectional lift coefficient |
| $C_T$ | Rotor thrust coefficient |
| $D$ | Finite-difference operator |
| $f=0$ | Function that describes the surface (i.e. the rotor blade). |
| $L_i$ | Components of loading acting on the fluid, Nm$^{-2}$ |
| $L_r$ | $L_i\hat{r}_i$, loading in the radiation direction (summation implied), Nm$^{-2}$ |
| $L_M$ | $L_i\hat{M}_i$ (summation implied), Nm$^{-2}$ |
| $\dot{L}_r$ | $\hat{r}_i\partial L_i/\partial t$ (summation implied), Nm$^{-2}$ s$^{-1}$ |
| $M$ | Local Mach number; Mach number of source in acoustics, $v/c$ |
| $M_i$ | Components of the Mach number of the acoustic source, $M_i = v_i/c$ |
| $M_r$ | $M_i\hat{r}_i$, Mach number of source in radiation direction (summation implied) |
| $p'$ | Acoustic pressure, $p-p_0$ in the undisturbed medium, Pa |
| $p'_T$ | Thickness contribution to $p'$, Pa |
| $p'_L$ | Loading contribution to $p'$, Pa |
| $R$ | Rotor radius, m |
| $r$ | Radial distance, distance between observer and source (equations 6 and 7), m |
| $\mathbf{r}$ | Position vector of collocation point, m |
| $\mathbf{r}_0$ | Initial position of collocation point, m |
| d$S$ | Element of the rotor blade surface, m$^2$ |
| $T$ | Rotor thrust, N |
| $t$ | Time, s |
| $U_n$ | Normal velocity of blade surface, ms$^{-1}$ |
| $\dot{U}_n$ | $\hat{n}_i\partial\hat{U}_i/\partial t$ (summation implied), ms$^{-2}$ |
| $U_{\dot{n}}$ | $U_i\partial\hat{n}_i/\partial t$ (summation implied), ms$^{-2}$ |
| $\mathbf{V}$ | Velocity vector at collocation point, ms$^{-1}$ |
| $x,y,z$ | Cartesian coordinates, m, m, m |

Greek

| | |
|---|---|
| $\gamma$ | Flight path angle, deg |
| $\Gamma$ | Circulation, m$^2$s$^{-1}$ |
| $\Delta t$ | Time step, s |
| $\Delta\psi$ | Azimuthal discretization, deg |
| $\Delta\zeta$ | Vortex age discretization, deg |
| $\zeta$ | Wake (vortex) age, deg |
| $\mu$ | Advance ratio |
| $\psi$ | Azimuth angle, deg |
| $\psi_b$ | Blade azimuthal location, deg |
| $\Omega$ | Rotor rotational speed, rad s$^{-1}$ |
| $\boldsymbol{\omega}$ | Vorticity, m$^2$s$^{-1}$ |
| $\rho_0$ | Density of quiescent medium, kg m$^{-3}$ |


[*]Graduate Research Assistant; chennes@psu.edu
[†]Graduate Research Assistant; huc115@psu.edu
[‡]Associate Professor; ksbrentner@psu.edu
[§]Graduate Research Assistant; shreyas@glue.umd.edu
[¶]Professor; leishman@eng.umd.edu



Presented at the AHS 4th Decennial Specialist's Conference on Aeromechanics, San Francisco, California, January 21–23, 2004.

## Introduction

Rotor noise alleviation has been a key area of rotorcraft research during the last two decades. Nevertheless, the accurate prediction of rotor noise remains a great challenge to the rotorcraft analyst. This is, in part, a result of deficiencies in modeling the rotor wake dynamics and associated induced inflow. The relatively poor performance of existing aerodynamic models, which may often be based on simple, steady momentum inflow assumptions, suggests that the computation of transient wake dynamics must be performed at a more rigorous, time-accurate level of approximation. The situation is particularly complicated in maneuvering flight, where the unsteady blade airloads and associated rotor noise change continuously throughout the maneuver. Thus, the transient wake aerodynamics need to be captured accurately and the noise must be computed over longer time-periods.

The objective of the current study is to investigate the influence of maneuvers and other transient rotor motion on the wake generated by a rotorcraft and, ultimately, on the noise generated. Although the present state-of-the-art is able to provide good predictions of rotor noise during steady rectilinear flight, this capability does not meet the challenge of real-world operations, which always include maneuvering flight. Recently Brentner *et al.*[1,2] have developed the PSU-WOPWOP code to investigate maneuvering rotorcraft noise, and as a preliminary step coupled it with the GENHEL rotorcraft flight dynamics code[3] to obtain the blade loading and aircraft motion data for the noise calculations. This preliminary work demonstrated that a rotorcraft may produce significantly more noise during a transient maneuver than during steady flight. The GENHEL code, however, uses a simple dynamic inflow model, which is incapable of modeling the significant rotor/wake interactions expected in many maneuver situations. These rotor/wake interactions plays a significant role in the noise generation, so the accuracy of the wake model is extremely important. In the present study, the time-accurate free-vortex wake method developed at the University of Maryland[4,5] is used to calculate the rotor wake and corresponding unsteady blade loads for several different maneuver cases. These loads are then used as input to calculate the noise produced during the maneuver.

## Impact of Transient Maneuver

A transient maneuver is a short-time event, typically initiated through pilot control, which significantly perturbs the rotor system from its steady-state operating condition. In particular, the blade motion and aerodynamic loading are aperiodic during a transient maneuver. This means that each rotor blade encounters a different aerodynamic environment during a single rotor revolution. Although a transient maneuver is short-time event, it typically requires that the aerodynamic response must be computed over many rotor revolutions. Similarly, the noise generated during the transient event continues to change over a relatively long time period* and may be highly directional. The aperiodic nature of the rotor response during a transient maneuver and the long time scales present significant new challenges to predicting both the rotor wake dynamics and the rotor noise.

## Maneuvering Wake Dynamics

The blade-wake interactions that occur on helicopter rotors can be very pronounced in many flight conditions. This is particularly significant in descending flight or in maneuvering flight, where the closer proximity of the wake to the blades can give rise to large unsteady airloads and the generation of impulsive rotor noise. Under nominally steady-state (non-maneuvering) flight conditions, the evolution of the rotor wake is periodic at the rotor rotational frequency. In this case, the rotor wake structure and the orientation of the tip vortices to the rotor blades are the same during each successive rotor revolution. However, this is not the case under transient maneuvering flight conditions, which produce an aperiodic wake structure. Flight maneuvers can also be associated with a significant, aperiodic reorganization of this wake structure, especially when the maneuver is abrupt or transient in nature.[6] Furthermore, as is typical of most unsteady aerodynamic effects, significant time-scales can be involved with the rotor wake reorganization during maneuvering flight conditions. This means that the rotor wake developments must be tracked (modeled) over very long times. This poses considerable challenges to the helicopter analyst—challenges that are yet to be satisfactorily resolved.

Physically, the rotor wake is comprised of vortex sheets generated at the trailing edge of the blades. These sheets, however, quickly roll-up into strong tip vortices, and become the dominant flow structures found inside the rotor wake. These discrete tip vortices not only affect rotor loads and performance, but are responsible for much of the rotor noise. Close interactions between the tip vortices and the blades, which are generally termed blade-vortex interactions (BVIs), generate highly unsteady aerodynamic loads, which are often very impulsive in nature. These impulsive airloads are the source of a particularly harsh obtrusive noise signature from the rotor. Therefore, the occurrence of any BVIs is relatively important from an overall rotor acoustics point of view. However, the specific magnitude and directivity of the rotor BVI noise is sensitive to both the position and aerodynamic structure of the tip vortices (i.e., their

*Long compared to a single blade passage period.

strength and induced velocity field) to the blades. Generally, BVIs that occur when the leading edge of the blade is nearly parallel to the longitudinal axis of the tip vortex are the most acoustically significant. However, interactions that occur with any relative orientation are aerodynamically significant.

To predict reliably both rotor airloads and acoustics during transient maneuvering flight, the dynamic evolution of the wake and the tip vortices needs to be modeled in a time-accurate manner throughout the maneuver. This often leads to wake developments that are relatively different to those expected on the basis of periodic flow assumptions. For example, it has been observed[7,8] that during a rapid change in the rotor operating conditions (such as with the use of abrupt collective or cyclic pitch inputs), the wake developments can be accompanied by the bundling of individual tip vortices. Periodic changes in blade pitch control inputs also produce changes in the wake structure, and can cause a continuous formation and propagation of accumulated bundles of wake vorticity. In the case of periodic collective pitch inputs, the wake vortices essentially form into a series of stacked toroidal vortex bundles. Whereas in the case of periodic cyclic inputs the bundles take on a more helicoidal form.[6] In some cases, transient effects lead to the formation of powerful toroidal "rings" of accumulated wake vorticity. These rings are spatially and temporally unstable, and break down as they are subsequently convected through the rotor wake.[9] In some cases, the blades may also interact with these bundles of vorticity, producing a form of "super" BVI. More importantly, however, in all cases there are considerable lags in the development of the rotor airloads, producing significant amplitude and the phasing effects on the unsteady blade loads compared to those obtained under steady flight conditions.

### Maneuvering Rotor Acoustics

Noise generation during a transient event is also significantly more complicated than during steady-state flight conditions. A transient maneuver typically results in a combination of transient and residual changes to the blade loading. These increases (or decreases) in loading directly affect the loading noise in an essentially linear manner. This is not the only effect on the transient noise, however. The aperiodic blade motion and the time rate of change of loading also have a strong impact on both the magnitude and directivity of the noise generated. The aperiodic blade motion will change both the acceleration and blade position relative to what would have occurred in the periodic case. Hence the thickness and loading noise are both affected. Additional unsteady loading will directly increase the loading noise, much like BVI. These effects can combine to magnify the impact a maneuver has on the rotor noise generation beyond what is expected if only the increase in load factor is considered.

In addition to the low frequency loading changes during the maneuver, the rotor wake is more likely to interact with the blades, resulting in forms of BVI. Under some circumstances these interactions produce extremely large amounts of noise, nearly overwhelming the other sources. In particular, when the interactions are parallel to the leading edge of the blade and thus occur over a relatively long time period and over a large area the noise is extremely loud. Recent transient wake computations[6] suggest that BVIs can be significantly increased in magnitude and extent during a maneuver. The present results are the first to investigate both the low frequency and BVI noise aspects of transient rotor maneuvers.

## Theory and Computational Approach

Although rotor aeroacoustic analyses have been performed with a wide variety of methods, most models assume or enforce periodicity of the wake solution. These analyses, therefore, lack the fundamental capability to properly predict noise under arbitrary maneuvering flight conditions. A more general method, capable of computing aperiodic solutions with considerable accuracy and fidelity, is clearly a prerequisite to obtain more accurate acoustic predictions.

### Free-Vortex Rotor Model

Under maneuvering flight conditions, the modeling of rotor airloads and the wake must be closely coupled and solved in a time-accurate sense to capture the transient wake evolution and its feedback effect on the unsteady rotor airloads and temporal blade response. This involves a numerical solution of the equations governing the wake development along with the simultaneous solution of the equations governing the blade dynamics. Most rotor wake models (e.g., Refs. 10–14) use either explicit or implicit periodicity assumptions, which are not suitable for transient maneuvering flight conditions. The situation is further complicated when predicting the acoustics of the rotor because of the extremely high spatial and temporal fidelity required to properly predict the BVI induced impulsive fluctuations on the rotor airloads.

Of all types of wake methods, free-vortex methods offer one of the best opportunities in predicting the time-dependent wake dynamics while still retaining acceptable levels of computational cost for routine use.[5] In a free-vortex model, the rotor wake is represented using discrete elements of vorticity. The elements are described by particle markers, which may be spatially contiguous or otherwise.[15] The method tracks these markers and their corresponding vorticity (circulations). The vortex filament method involves a discretization of wake vorticity into straight-line segments connected by a series of markers, one at each end of the filament. This is the approach used in the present work.

The development of the wake is described in three-dimensional, incompressible, viscous flow by the Navier-Stokes equations. These can be expressed in a velocity-vorticity $(\mathbf{V},\boldsymbol{\omega})$ formulation as

$$\frac{d\boldsymbol{\omega}}{dt} \quad = \quad -(\mathbf{V}\cdot\nabla)\boldsymbol{\omega}+(\boldsymbol{\omega}\cdot\nabla)\mathbf{V}+\nu\Delta\cdot\boldsymbol{\omega} \qquad (1)$$

In free-vortex filament methods, the vortex elements are assumed to be singular filaments of constant circulation. In this case, the governing equation for the wake becomes the simpler advection (convection) equation

$$\frac{d\mathbf{r}}{dt}=\mathbf{V}(\mathbf{r},\mathbf{t}), \quad \mathbf{r}(\mathbf{t}=\mathbf{0})=\mathbf{r_0} \qquad (2)$$

where $\mathbf{r}$ is the position vector of a point on the vortex filament, $\mathbf{r_0}$ is the initial position vector, and $\mathbf{V}$ is the local velocity field at that point. Because the position vector $\mathbf{r}$ is a function of both blade position, $\psi$, and the time after which it was trailed into the wake, this equation applies to each and every marker. In blade fixed coordinates the foregoing equation can be written as the partial differential equation

$$\frac{\partial\mathbf{r}(\psi,\zeta)}{\partial\psi}+\frac{\partial\mathbf{r}(\psi,\zeta)}{\partial\zeta}=\frac{1}{\Omega}\mathbf{V}(\mathbf{r}(\psi,\zeta)) \qquad (3)$$

In discretized form, equation 3 can be written as

$$\frac{\partial\mathbf{r}}{\partial\psi}+\frac{\partial\mathbf{r}}{\partial\zeta}\approx D_\psi+D_\zeta=\sum V \qquad (4)$$

where $D_\psi$ is the spatial finite-difference operator and $D_\zeta$ is the temporal operator, using discretizations $\Delta\psi$ and $\Delta\zeta$, respectively. All of the present calculations were done using a discretization of $\Delta\psi=\Delta\zeta=2.5\,$deg. The right-hand side of the foregoing equation, $\sum V$, represents a general summation of the induced velocity effects from all of the vortical elements in the flow field, including the rotor wake. This term is obtained numerically through the repeated use of the Biot-Savart law[16] applied to all of the discrete filaments, followed by numerical summation of the induced velocity effects.

The resulting finite-difference equation, which applies to each and every marker in the wake, is then solved numerically in space and time.[4,5] Special numerical techniques are used to provide stability to the method for time-marching solutions, while still retaining the order of accuracy. During the convection process, the vortex filaments are also allowed to stretch and diffuse under the action of viscosity. These effects are accounted for in the free-vortex model by using a viscous splitting approach.[17]

The wake solution is intrinsically coupled with the blade aerodynamics and the dynamic flapping response of each blade.[18] This response becomes aperiodic in time during maneuvering flight. Therefore, the time-varying blade aerodynamics and the resulting dynamic responses of each blade must be solved simultaneously, and to a consistent level of accuracy. These equations were integrated using the same numerical scheme employed in solving the governing equations of the wake.

In the present case, the rotor was modeled with elastically stiff blades, each of which execute fully independent and time-dependent flapping motion. Aerodynamically, each blade was modeled using a Weissinger-L lifting-surface model,[19] where the blade was divided into 32 spanwise blade elements. The strength of the bound circulation was assumed to remain constant over each blade segment, and vorticity, equal to the difference in bound circulation strengths between two adjacent segments, was trailed into the wake behind each blade. This constitutes the near-wake behind the blade, which then forms a boundary condition for the rolled-up free-vortex representation of the rotor wake.

The unsteady aerodynamics on the blades were calculated using the indicial response method,[20,21] which was applied at each blade element. The ability to handle completely arbitrary aerodynamic conditions at the blade gives the indicial approach considerable flexibility in meeting the requirements of this type of aperiodic rotor airloads analysis. From the calculated blade element airloads the rotor thrust was calculated by radial and azimuthal integration.

## Rotor Noise Model

The PSU-WOPWOP rotor noise prediction code[1] is used in this work to predict the main rotor noise in both steady and transient maneuver flight conditions. This code is an implementation of Farassat's retarded-time formulation 1A of the Ffowcs Williams-Hawkings (FW-H) equation:[22,23]

$$p'(\mathbf{x},t)=p'_T(\mathbf{x},t)+p'_L(\mathbf{x},t) \qquad (5)$$

where the thickness noise contribution $p'_T$ is defined as

$$\begin{aligned}4\pi p'_T(\mathbf{x},t)= &\int_{f=0}\left[\frac{\rho_0(\dot{U}_n+U_{\dot{n}})}{r(1-M_r)^2}\right]_{\rm ret}dS\\ &+\int_{f=0}\left[\frac{\rho_0 U_n(r\dot{M}_r+c(M_r-M^2))}{r^2(1-M_r)^3}\right]_{\rm ret}dS\end{aligned} \qquad (6)$$

and the loading noise contribution $p'_L$ is defined as

$$
\begin{aligned}
4\pi p'_L(\mathbf{x},t) = \quad & \frac{1}{c}\int\limits_{f=0} \left[\frac{\dot{L}_r}{r(1-M_r)^2}\right]_{\text{ret}} dS \\
& + \int\limits_{f=0} \left[\frac{L_r - L_M}{r^2(1-M_r)^2}\right]_{\text{ret}} dS \qquad (7) \\
+\frac{1}{c}\int\limits_{f=0} & \left[\frac{L_r\left(r\dot{M}_r + c(M_r - M^2)\right)}{r^2(1-M_r)^3}\right]_{\text{ret}} dS
\end{aligned}
$$

The FW–H quadrupole term, which is necessary for the prediction of high-speed impulsive noise, has been neglected. In Eq. 6, maneuver influences the thickness noise through the normal component of the blade surface velocity, $U_n$, and its time derivative $\dot{U}_n + U_{\dot{n}}$ These velocity components must represent both the periodic and aperiodic rotor blade motion combined with the aircraft motion. In this work, GENHEL provided the full set of parameters needed to compute the position, velocity, and acceleration of the rotor blade surfaces. PSU-WOPWOP reconstructs the rigid body motion of the blades.

A transient maneuver also influences the rotor noise through the blade loading $L_i$ and its time derivative $\dot{L}_i$in Eq. 7. The loading noise is assumed to be compact in the chordwise direction (i.e., the wavelength is large compared to the chord). This approximation (which is valid up to about the 35th harmonic of rotor blade passage frequency for the rotor used here) enables the noise prediction to use the integrated section loading rather than a pressure distributed over the actual blade surface. Both GENHEL and the free-vortex model compute only integrated, sectional rotor loading for each blade as a function of span and time (azimuth).

Although Farassat's formulation is a retarded time formulation, there are several possible methods of numerical implementation. For a transient maneuvers, in which there are many coordinate systems used in the position and motion calculations, it is computationally efficient to use a source-time dominant solution method.[1,24,25] In this method, the source time is chosen first, then the time at which the sound from a single point on the source surface reaches the observer is then computed. The noise signal from each point on the source surfaces (rotor blades) is interpolated at constant observer times so that the signals can be added together, hence providing the complete acoustic pressure time history.

## Analysis of Transient Maneuvers

Three transient maneuvers have been evaluated for an aircraft which is representative of a utility transport helicopter: "pop-up," "pop-down," and arrested descent. The helicopter is a single-rotor / tail-rotor configuration with an articulated horizontal stabilizer. The main rotor

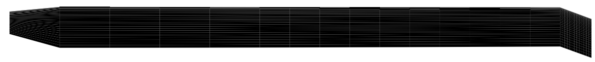

Figure 1: Main rotor planform of utility transport helicopter used in this study.

is a four-bladed articulated rotor with swept blade tips, as shown in Fig. 1. The tail rotor is modeled using a simplified "Bailey" solution in GENHEL for the flight dynamics simulation. The tail rotor is not included in either the free-vortex model or in the noise prediction. The aircraft includes basic electronic stability augmentation in the roll, pitch, and yaw axes. In order to simulate basic maneuvers without a pilot in the loop, an outer loop controller was used. A description of key aircraft parameters used in the flight simulation is given in Table 1.

For the maneuver analyses, the control inputs, aircraft roll, pitch and yaw angles, and helicopter position were computed with the GENHEL simulation and then passed to both the free-vortex model and PSU-WOPWOP. The flight simulation was performed by first trimming the helicopter to the desired steady flight condition (hover or forward flight), and then initiating the maneuver with the use of a pilot controls. The GENHEL computations were conducted for a simulated time period of 2 seconds (approximately 10 rotor revolutions). The free-vortex model, however, was run for longer periods of simulated time to observe any transients in the wake evolution well after the control inputs were restored to their original conditions. During this period, the control inputs and the flight conditions (velocities and angular rates) were set to the final values predicted by GENHEL. The noise prediction is the final stage of the analysis. The unsteady rotor loading from either GENHEL or the free-vortex rotor model can be used in PSU-WOPWOP for the rotor noise prediction.

### "Pop-up" Maneuver

In a pop-up/down maneuver the pilot starts from a hovering condition and applies a rapid collective pitch input to perform a near-vertical ascent or descent. Fig-

Table 1: Description of utility transport helicopter used in current study.

| | |
|---|---|
| Aircraft weight | 74,841 N |
| Rotor radius | 8.177 m |
| Nominal rotor speed | 258 rpm |
| Radius of tip sweep | 95% |
| Tip sweep angle | 20° |

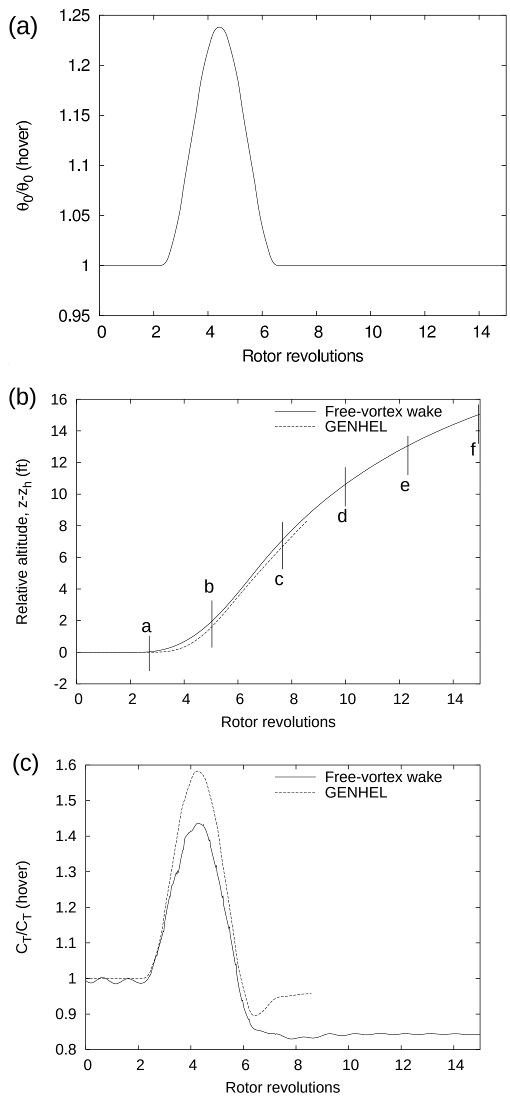


Figure 2: Collective pitch perturbation and the time-history of the rotor thrust for a hovering rotor undergoing pop-up maneuver. (a) Collective pitch relative to the hover value, (b) Altitude, (c) Rotor thrust coeffi cient.

ures 2(a)–(c) show the relative change in the collective pitch control setting for a pop-up maneuver, the altitude as climbing occurs, and the rotor thrust time-history. In this case, a positive collective pitch input was applied in the form of a half-doublet over a period of approximately five rotor revolutions. Notice that both GENHEL and the free-vortex method are in good agreement in terms of the overall behavior of the rotor thrust and the climb response (altitude). The differences in rotor thrust arise mainly from the different modeling of the wake dynamics. Notice also that the results from GENHEL and the free-vortex model do not return to their initial values at the end of the maneuver. This is because the GENHEL simulation needs to be carried out to a longer period of time for fully trimmed hovering flight conditions to be reestablished.

Figure 3 shows the snapshots of the side view of the rotor wake as predicted with the free-vortex model at different instants in time during the pop-up maneuver. These times are identified by the labels (a)–(f) in Fig. 2(b). Figure 3(a) shows the wake geometry at the instant just before the collective control input was applied. The wake geometry here is essentially periodic. After the collective pitch was increased, however, the tip vortices were noticed to pair up in the wake below the rotor to form a toroidal vortex bundle or "ring" – see Ref. 6 for a detailed discussion of this effect. This vortex bundle then begins to propagate downward through the wake away from the rotor – see Fig. 3(b). Figure 3(c) shows the wake structure at five rotor revolutions after the control inputs were restored to their initial values. Clearly, the wake has not yet returned to its periodic operating state. Figures 3(d)-(f) show snapshots of the wake geometry after the maneuver inputs have been completed. Notice that the vortex bundle eventually convects out of the rotor flow field, and the wake returns to its original undisturbed state.

The acoustic pressure time history for an observer located $3.73R$ below the rotor and $6.12R$ from the rotor axis at $t = 0$ using data from both GENHEL and the free-vortex wake simulation is shown in Fig. 4. In this case the results match quite well because any BVI occurrences are nearly perpendicular to the rotor blades rather than the more acoustically significant case of a parallel BVI interaction. Hence the results from the dynamic inflow model used by GENHEL are not substantially different from those computed with the free-vortex model for this maneuver.

The acoustic field generated during the pop-up maneuver is essentially axisymmetric; therefore, only the noise on a radial line extending $12.23R$ from the main rotor axis has been plotted. Figure 5 shows the overall sound pressure level (OASPL) on a radial line $3.73R$ below the rotor as a function of time as computed from the free-vortex model. All of the OASPL calculations shown in the present paper were made using a 0.2s Hanning window followed by the addition of a 4.26dB broadband correction factor.† The increase in noise as the collective increases is clearly visible beginning directly below the rotor and propagating outward. This is seen on the plot as a slight upward angle because of the finite speed of sound. As the collective is decreased at the end of the maneuver the OASPL decreases, as expected for this type of maneuver.

†A Hanning window is applied because the signal is not periodic, but the application of the Hanning window results in a loss. For a broadband signal the resultant spectral density is multiplied by a factor of $\sqrt{8/3}$, i.e., an addition of 4.26dB.[26]

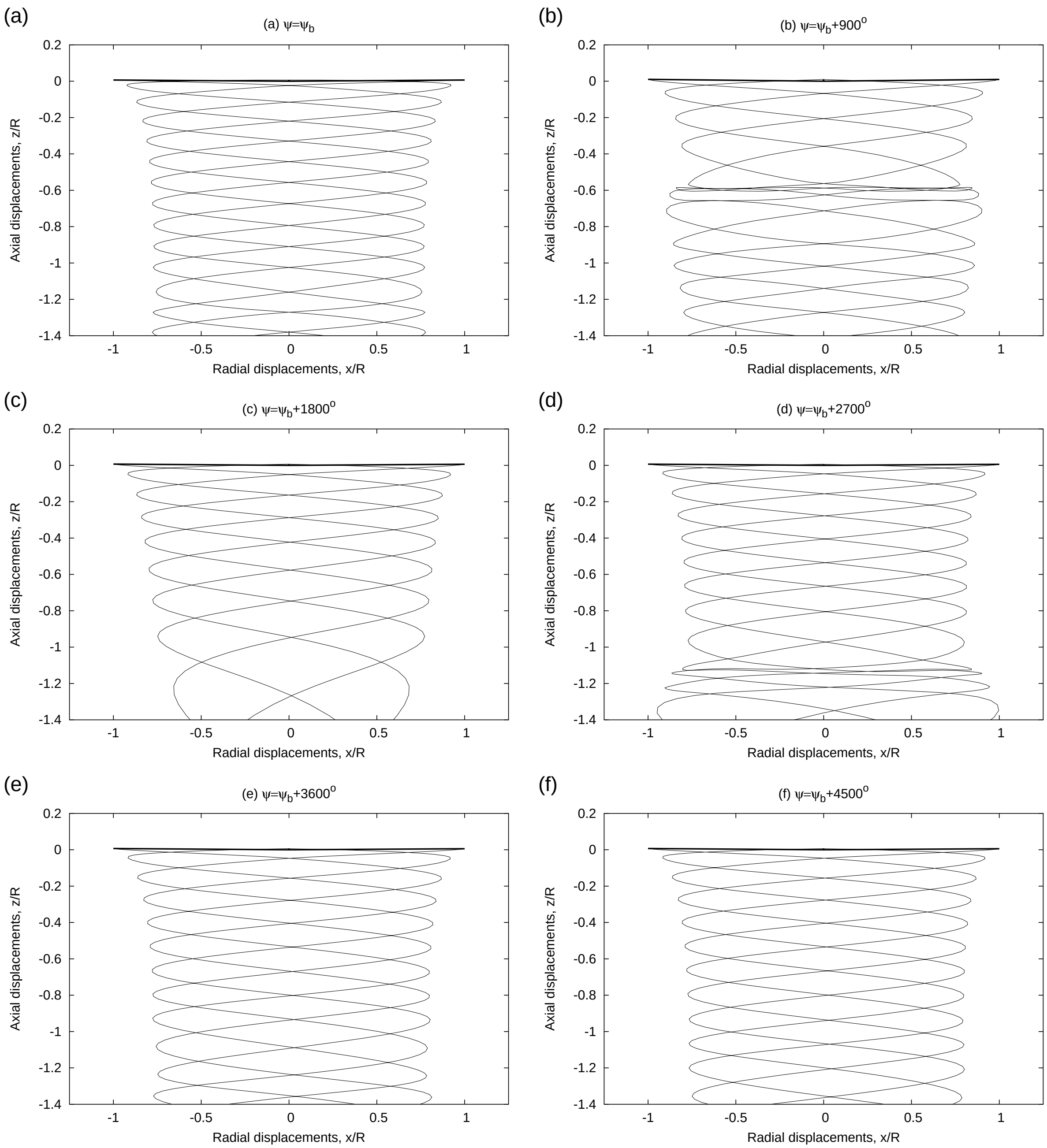


Figure 3: The side view of the free-vortex wake geometry of a hovering rotor undergoing pop-up maneuver at various instances in time. (a) Steady periodic condition, (b) Maximum collective pitch, (c) Collective pitch restored to initial value, (d) 7.5 rotor revolutions after initiating the maneuver, (e) 10 rotor revolutions after initiating the maneuver, (f) Wake returns to nominally periodic conditions.

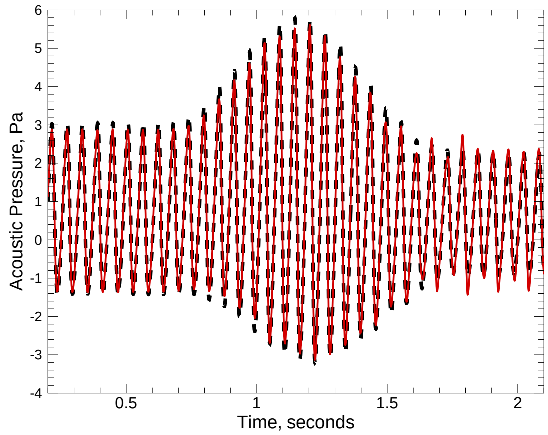


Figure 4: Acoustic pressure time history of the pop-up maneuver for an observer located 3.73$R$ below the rotor and 6.12$R$ from the rotor axis at $t = 0$. – – – GENHEL loading; ——— free-vortex wake model loading.

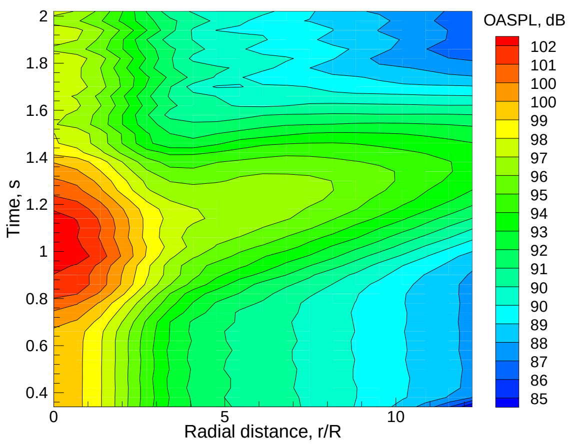


Figure 5: OASPL time history for the pop-up maneuver for a line of observer locations extending 12.23$R$ from the rotor axis on a plane 3.73$R$ below the helicopter at $t = 0$.

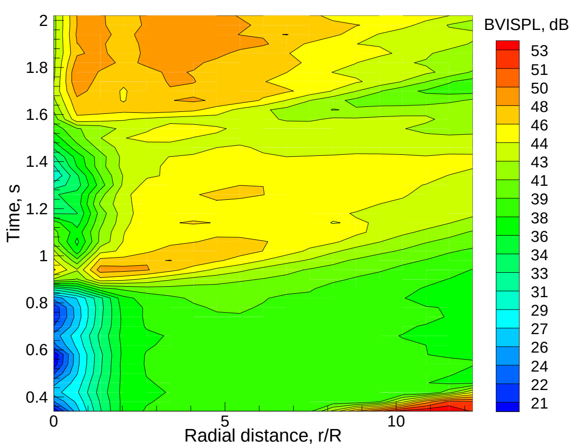


Figure 6: BVISPL (7th – 50th harmonics of blade passage period) time history for the pop-up maneuver for a line of observer locations extending 12.23$R$ from the rotor axis on a plane 3.73$R$ below the helicopter at $t = 0$.

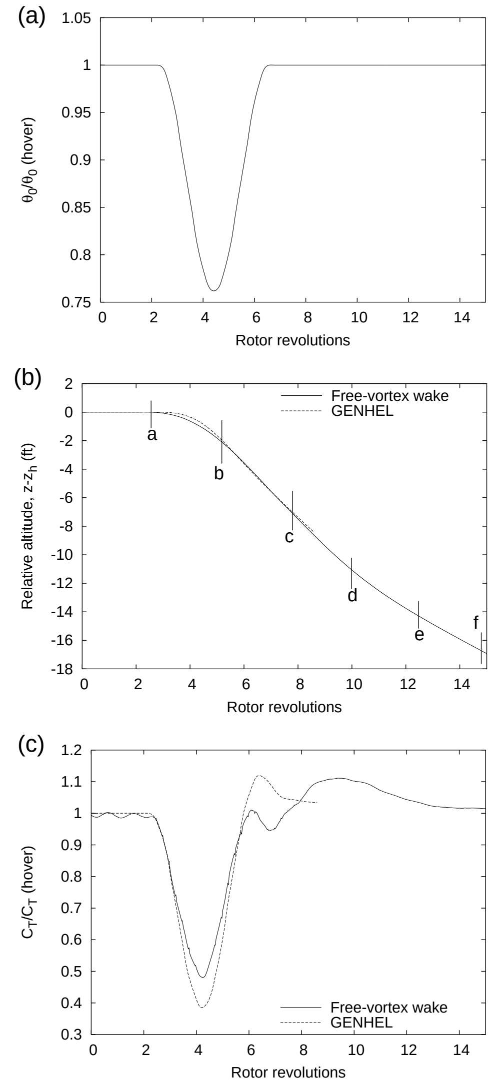


Figure 7: Collective pitch perturbation and the time-history of the rotor thrust during pop-down maneuver. (a) Collective pitch, (b) Altitude, (c) Rotor thrust coeffi cient.

Figure 6 shows the BVI sound pressure level (BVISPL) as a function of time on the same radial line. The BVISPL is calculated by summing the 7th through 50th harmonics of the blade passage frequency, which is the frequency range in which BVI noise is expected to have the most influence. In the pop-up case nearly all of the noise generated is low frequency noise, as can be seen by comparing the OASPL and BVISPL contours (Fig. 5 and 6). Although the human ear is less sensitive to the low frequency noise than to the higher-frequency BVI noise, low frequency noise is important for detectability considerations because low frequency noise is not attenuated by the atmosphere as easily as is higher frequency noise.

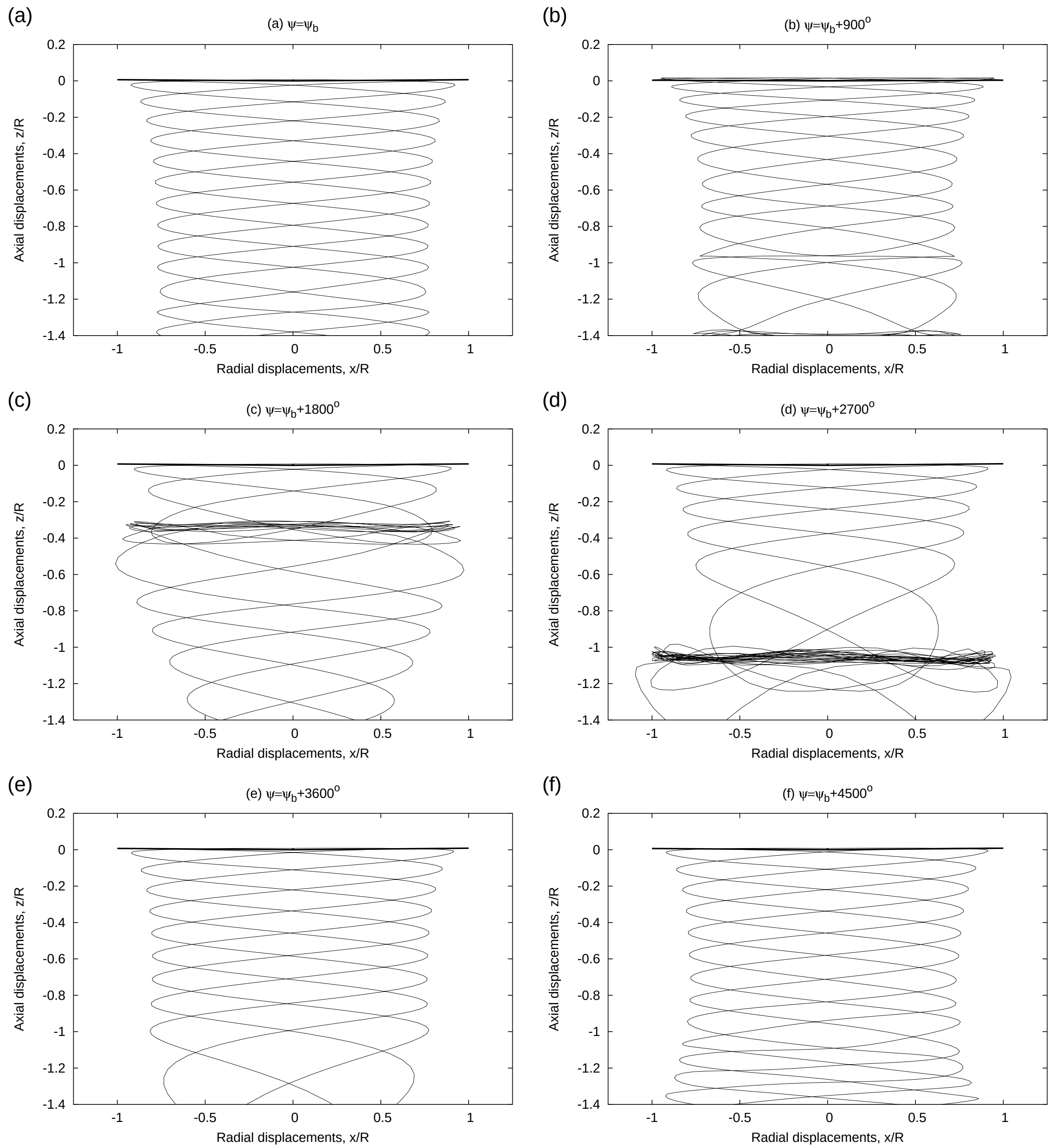


Figure 8: The side view of the free-vortex wake geometry of a hovering rotor undergoing pop-down maneuver at various instances in time. (a) Steady periodic condition, (b) Maximum collective pitch, (c) Collective pitch restored to initial value, (d) 7.5 rotor revolutions after initiating the maneuver, (e) 10 rotor revolutions after initiating the maneuver, (f) Wake returns to periodic conditions.

## “Pop-down” Maneuver

The pop-down maneuver is essentially the inverse of the pop-up maneuver. Figure 7 shows the control inputs, altitude and thrust time-history for the simulated pop-down maneuver. This case is important because the rotor now descends into its own wake, thereby enhancing the potential of BVI occurrences at the rotor disk. Once again, both GENHEL and free-vortex model predict similar overall results for the rotor thrust and rate of descent, but the behavior of the thrust is again slightly different. This difference, like in the case of a pop-up maneuver, can be attributed mostly to the effects of the rotor wake dynamics.

Figure 8 shows the snapshots of the side view of the free-vortex wake at various instances in time after the control inputs were applied, as marked by (a)–(f) in Fig. 7(b). In this case, the rotor descends and begins to encounter its own self-generated wake. This is apparent from Fig. 8(b), where the tip vortices generated at early wake ages can be seen to lie above the rotor tip-path-plane. The formation of a characteristic toroidal vortex bundle in the rotor wake can again be observed in Figs. 8(c) &(d). However, in this case the vortex bundle starts to form well below the rotor in the far wake. It then starts moving vertically upwards toward the rotor as the descent rate increases.

This interesting wake behavior is related to the relative helical pitch of the tip vortices and their strengths, and the effect on the overall stability of the rotor wake.[4,9] In this case, wake instabilities in the form of vortex pairing occurs in the far wake. The pairing leads to vortex bundling. After the collective pitch is restored to its initial value, the rotor thrust begins to stabilize and the vortex bundle is convected downstream away from the rotor. Periodic flow conditions are finally established, but only after at least 8 rotor revolutions after the collective pitch was returned to its initial condition. Notice that the upward/downward movement of the vortex bundle in the rotor wake is responsible for a second saddle in the thrust time-history, a result that is not predicted by GENHEL.

It was apparent that in the present pop-down maneuver simulation, the conditions were not sufficient to convect the accumulated vortex bundle structure up into the rotor tip-path-plane. It can, however, be expected that for certain magnitudes of control input perturbations and helicopter response, the vortex bundle will actually convect into the rotor plane and so cause large fluctuations in rotor airloads, which might be thought of as a “super” BVI.

The OASPL values computed from the free-vortex model are shown as a function of time on a radial line $3.73R$ below the rotor at $t = 0$ in Fig. 9. As in the pop-up case, the OASPL correlates closely with the collective pitch and rotor thrust coefficient, although as the helicopter nears the observer plane the levels increase

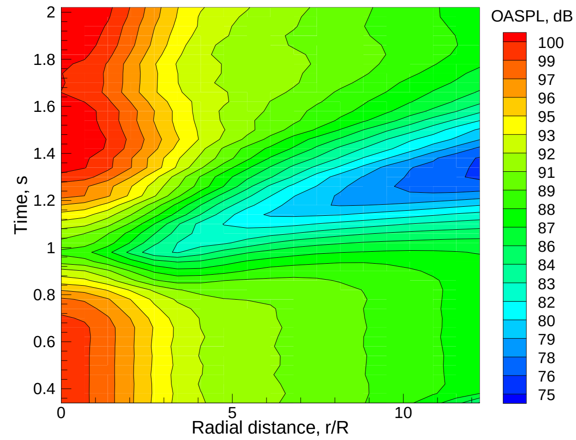


Figure 9: OASPL time history for the pop-down maneuver for a line of observer locations extending $12.23R$ from the rotor axis on a plane $3.73R$ below the helicopter at $t = 0$.

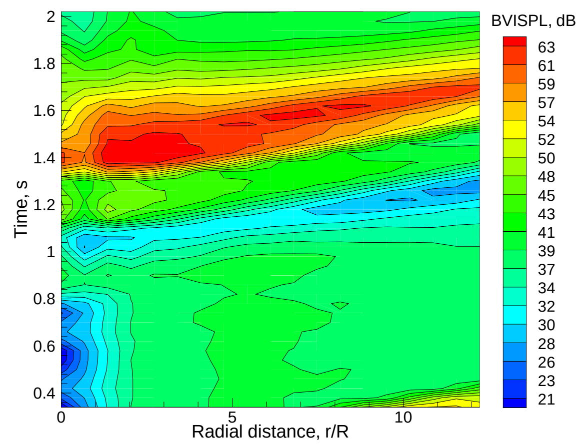


Figure 10: BVISPL (7th – 50th harmonics of blade passage period) time history for the pop-down maneuver for a line of observer locations extending $12.23R$ from the rotor axis on a plane $3.73R$ below the helicopter at $t = 0$.

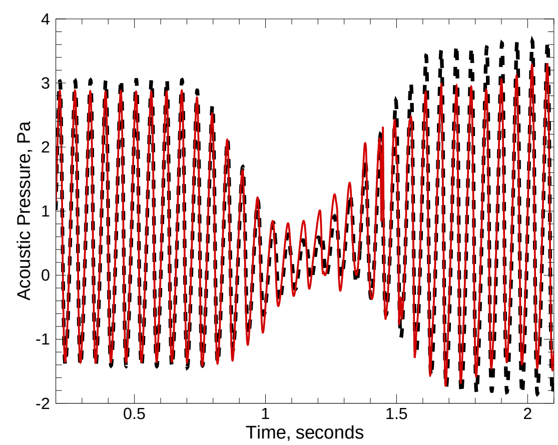


Figure 11: Acoustic pressure time history of the pop-down maneuver for an observer located $3.73R$ below the rotor and $6.12R$ from the rotor axis at $t = 0$. – – – GENHEL loading; ——— free-vortex wake model loading.

somewhat. Figure 10 shows the BVISPL on the same radial line. In this case, as in the pop-up maneuver, the BVISPL is much lower than the OASPL, indicating that most of the noise is at low frequencies. Figure 11 shows the acoustic pressure time history for an observer located 3.73$R$ below the rotor and 6.12$R$ from the rotor axis at $t = 0$ using airloads data from both GENHEL and the free-vortex wake simulation. The divergence near the end of the maneuver is because of a difference in inflow distribution, giving the free-vortex wake case higher loading at the blade tips, which are acoustically more important than at the inboard sections of the blade.

While constituting a simple maneuver from the pilot's point of view, pop-up and pop-down maneuvers demonstrate the sensitivity of the rotor wake to perturbation of control inputs and its influence on the rotor wake developments. However, in axial flight the BVIs are nearly perpendicular to the blades because the tip vortices are nearly helical in form below the rotor and so are not as acoustically significant.

## Arrested Descent Maneuver

In an arrested descent (or pull-up) maneuver, the pilot stops or "arrests" the steady descent the rotorcraft through a combination of pilot controls. For the simple maneuver examined here, the rotor was first trimmed for a steady, descending flight condition with a flight path angle, $\gamma = 6^\circ$ at an advance ratio, $\mu = 0.186$. The maneuver was performed by introducing a half-doublet input in collective pitch for a period of approximately five rotor revolutions – see Fig. 12. During this period there is an increase in the rotor thrust, which serves to arrest the rate of descent of the helicopter. The pilot input model also adjusted the tail rotor settings to maintain yaw equilibrium.

Low-speed, descending, forward-flight conditions are highly conducive to the development of BVIs. In low-speed flight, the tip vortices persist below the rotor, and the more skewed nature of the wake brings about BVIs over the rotor disk that are more acoustically significant. At certain rates of descent, the wake vortices can pass up through the rotor plane, thereby greatly enhancing the number and the intensity of the BVIs. Control input perturbations initiated in this flight condition can, therefore, be expected to cause further fluctuations in the wake development and changes in the BVI locations and orientations. This can be expected to have an impact on the rotor aeroacoustics.

Figures 13 & 14 show the snapshots of the wake dynamics at various instances in time during the pull-up maneuver. Figures 13(a) and 14(a) shows the baseline wake geometry when the helicopter is in the initial steady descending flight condition. At this point the collective pitch was increased to initiate the maneuver. Figures 13(b) and 14(b) shows the wake geometry when the applied collective pitch reaches a maximum. Notice that the tip-path plane is now also tilted backwards. This happens because of the dynamic effects on the rotor flapping response. It is apparent that the wake geometries in the two conditions (steady baseline and during the maneuver) are quite different, especially near the tip-path-plane of the rotor. The wake geometry only slowly returns to the steady baseline condition over the next 10 rotor revolutions after the collective pitch was restored to its initial condition – see Figs. 13(d)–(f) and 14(d)–(f).

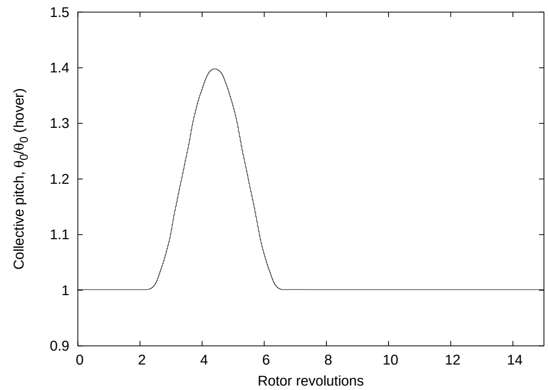

Figure 12: Plot showing the collective pitch input applied to perform an arrested descent maneuver.

The acoustic field is modified during the maneuver directly through the change in loading that results from the strong BVI. Figure 15 shows the normal force/unit span on the first rotor blade for several rotor revolutions during the arrested descent. The BVI is evident at locations on the rotor disk where loading changes rapidly (i.e., the loading contours are close together). This occurs on both the advancing and retreating sides of the rotor disk. Figure 15(a) is representative of the steady descent case, showing weak advancing-side BVI and very strong retreating-side BVI. As the maneuver begins, the character of the BVI changes: the retreating side BVI weakens and the advancing side BVI becomes much stronger. The rotor loading distribution has not completely returned to the steady-state condition by the 8th rotor revolution in Fig. 15(f).

Figure 16 shows the nondimensional sectional blade lift as a function of the rotor azimuth over a period of one rotor revolution for the arrested descent maneuver for the time when the collective pitch reaches a maximum. The results are compared with the baseline steady descent flight condition to quantitatively illustrate the effect of the wake dynamics on the rotor airloads. Results for three different blade spanwise locations are shown to illustrate the three-dimensional influence of the rotor wake.

It is apparent that the BVIs manifest as impulsive fluc-

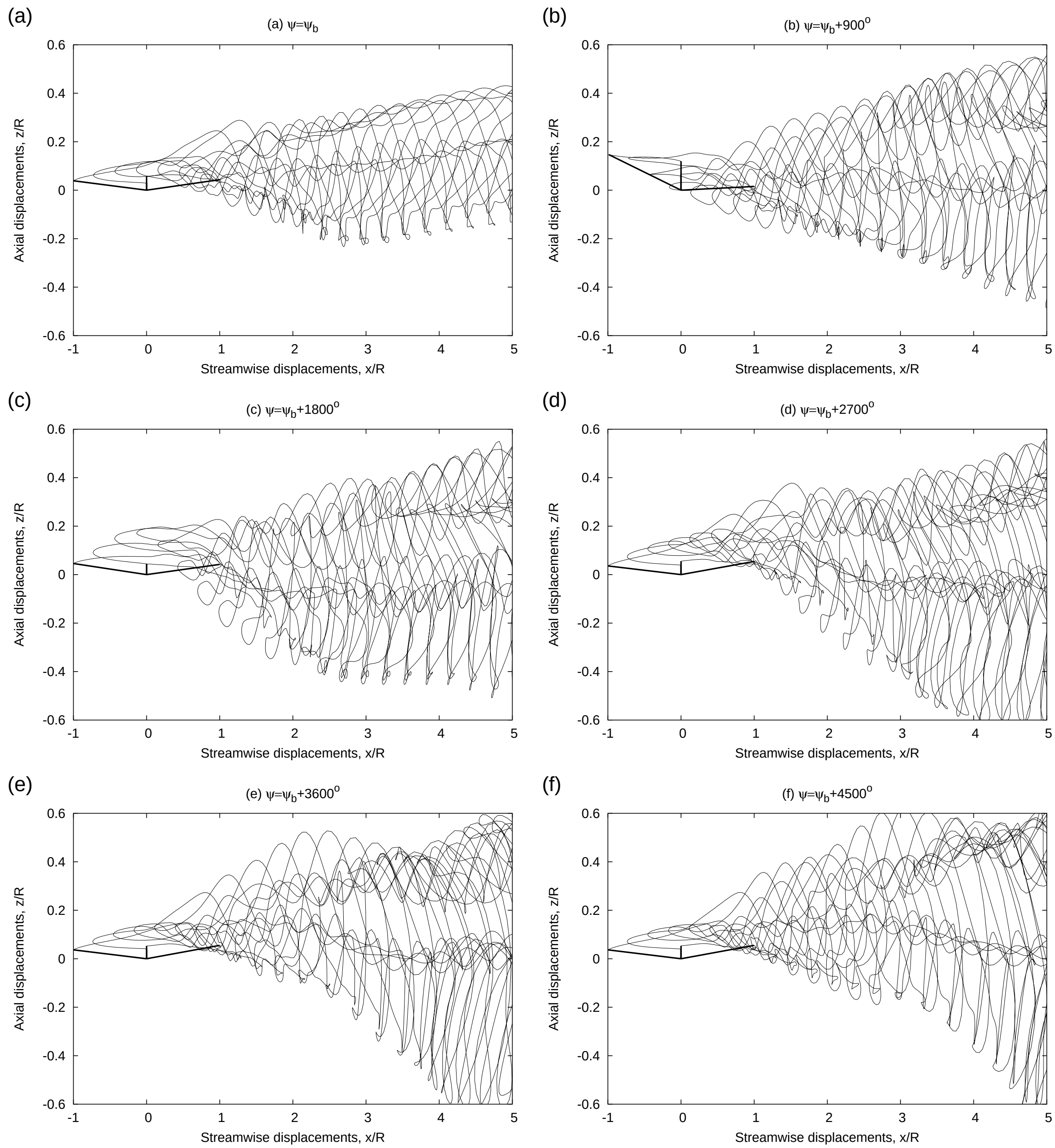


Figure 13: The side view of the free-vortex wake geometry of a rotor undergoing arrested descent maneuver at various instances in time. (a) Steady periodic condition, (b) Maximum collective pitch, (c) Collective pitch restored to initial value, (d) 2.5 rotor revolutions after maneuver, (e) 5 rotor revolutions after maneuver, (f) 7.5 revolutions after maneuver. $\mu = 0.186, \gamma = 6^\circ$.

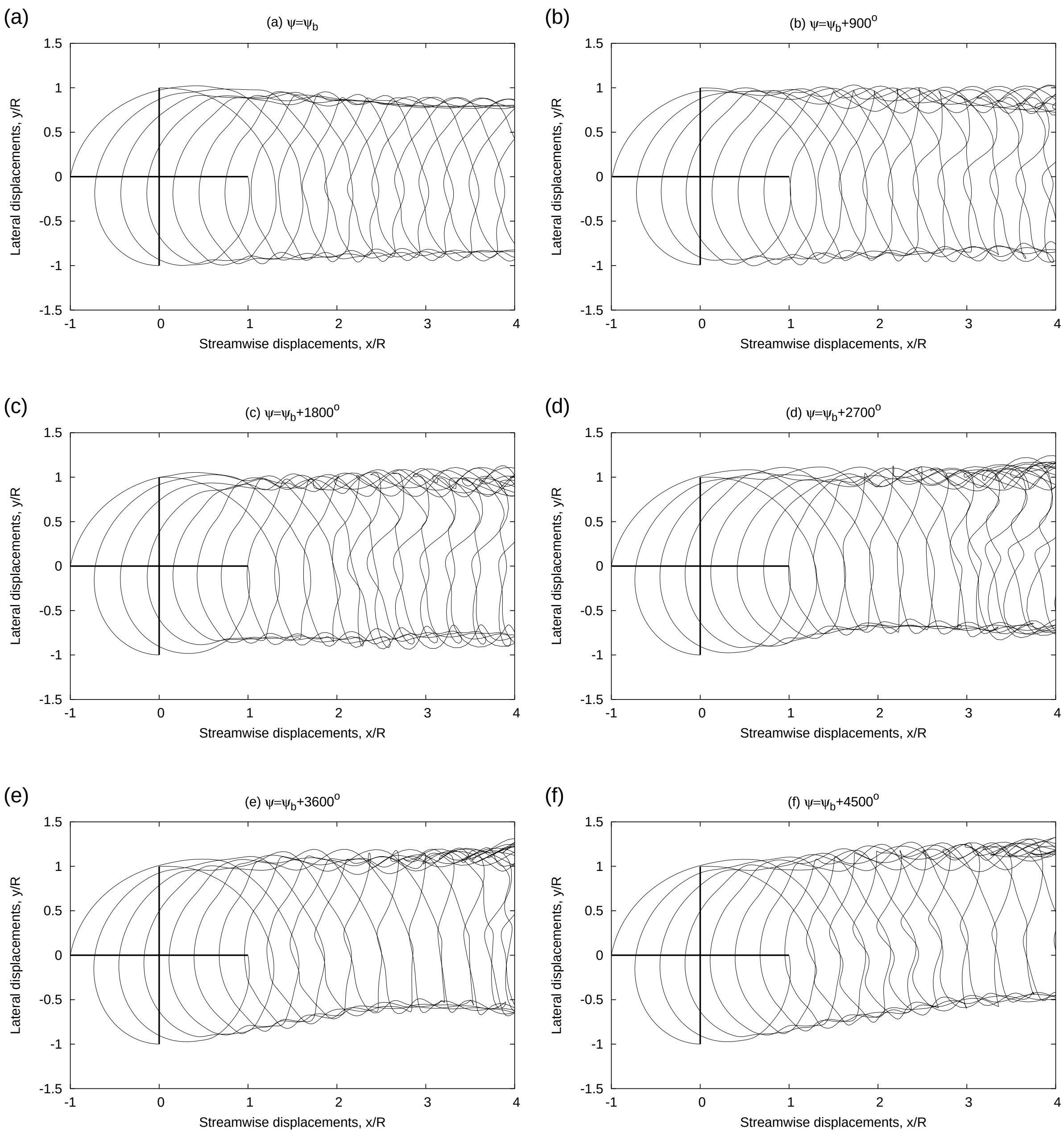


Figure 14: The top view of the free-vortex wake geometry of a rotor undergoing arrested descent maneuver at various instances in time. (a) Steady periodic condition, (b) Maximum collective pitch, (c) Collective pitch restored to initial value, (d) 2.5 rotor revolutions after maneuver, (e) 5 rotor revolutions after maneuver, (f) 7.5 revolutions after maneuver. $\mu = 0.186, \gamma = 6^{\circ}$.

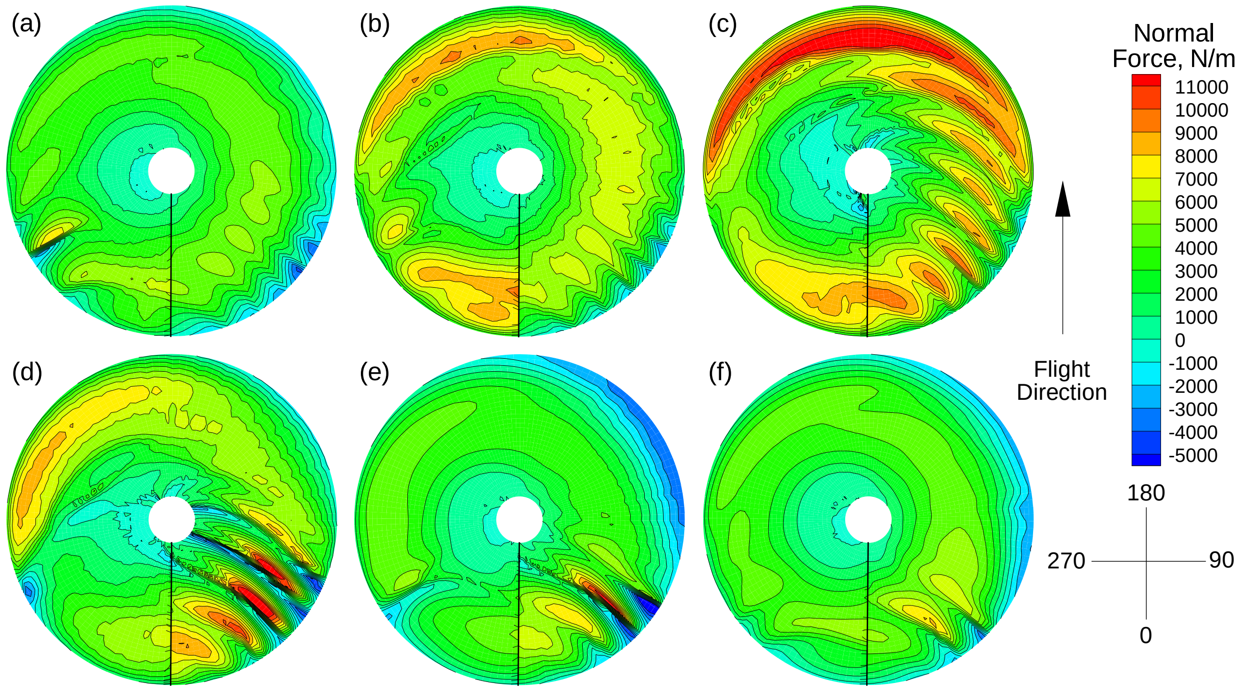


Figure 15: Section normal force on the reference blade as a function of rotor span and azimuth during the arrested descent maneuver. (a) rotor revolution 3; (b) rotor revolution 4; (c) rotor revolution 5; (d) rotor revolution 6; (e) rotor revolution 7; (f) rotor revolution 8.

tuations on the advancing and retreating sides of the rotor disk, but they are only acoustically significant when the interaction is nearly parallel to the rotor blade (i.e., $\psi = 30^\circ$ to $90^\circ$ and the advancing side and $\psi = 270^\circ$ to $330^\circ$ on the retreating side). In addition to the increase in mean value of lift, which is a direct consequence of the increased rotor thrust, the lift distribution (Fig. 16), also shows the differences between the two extremes of this maneuver.

The impact of BVI loading has a very strong impact on the noise generated by the rotor. When BVI noise exists, it is one of the most annoying sources of rotorcraft noise. This is demonstrated in a comparison of the noise computed from the GENHEL loading (which does not include BVI) and the free-vortex model, as shown Fig. 17. In this figure, the acoustic pressure is computed at a point near the typical maximum BVI noise location. While the GENHEL solution captures the nonimpulsive nature of the rotor noise, only the more rigorous, time-accurate free-vortex model captures the BVI noise. The peaks from BVI are clearly evident, and constitute the primary source of noise at this observer location.

The acoustic field generated by the rotor during the arrested descent maneuver is shown in Figs. 18 and 19. In these figures the OASPL and BVISPL contours are plotted for several representative times evenly spaced from the beginning of the maneuver to near the end of the maneuver. The OASPL and BVISPL contours are computed on a plane located 3.73$R$ below the rotor at $t = 0$. As the helicopter descends closer to the plane the OASPL increases slightly because of the decreasing distance. Throughout the maneuver, OASPL and BVISPL contours are very similar in shape and maximum levels. This indicates that the BVI noise dominates the noise spectrum in the areas of peak noise. Away from the peaks, the OASPL levels are somewhat higher because of the contribution of low-frequency noise.

In Figs. 18(a) and 19(a), which is essentially that of the steady descent case, retreating-side BVI noise is evident in the BVISPL and OASPL contours as a peak near the location $x/R = 0$, $y/R = -1$ and advancing side BVI noise can be seen near $x/R = 5$, $y/R = -3$. At this time the retreating-side BVI is dominant, as would be expected by an inspection of the blade loading in Fig. 15(a). As the maneuver proceeds, the combination of dramatic loading and tip-path-plane orientation changes results in the directivity change shown in Figs. 18 & 19. The retreat-side BVI noise disappears and the advancing-side BVI noise increases by about 10 BVISPL dB. As the maneuver nears completion, the acoustic field returns toward the initial condition.

It is also interesting to examine how the acoustic pressure changes at an observer position 3.73$R$ below the rotor's initial position, 4.59$R$ ahead, and 4.59$R$ on the advancing side, shown in Fig. 20. This observer position is in the region of maximum advancing-side BVI and acoustic pressure has been computed for both the GENHEL (no BVI) and free-vortex wake loadings. As

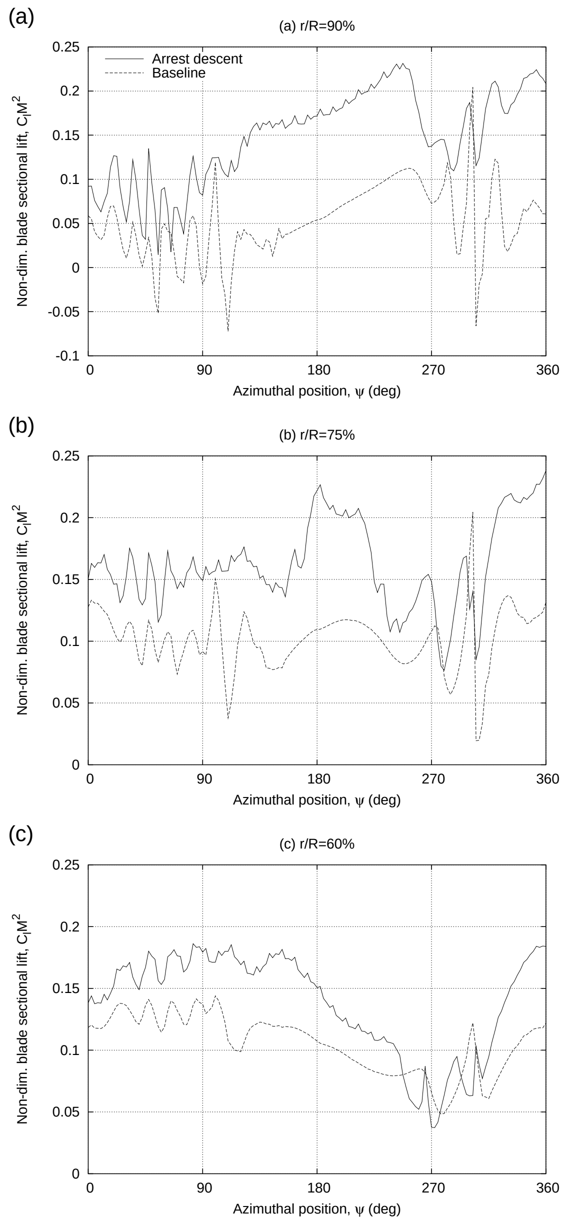


Figure 16: Comparison of azimuthal variation of the spanwise blade aerodynamic lift for a helicopter undergoing arrested descent maneuver in comparison to the baseline steady descending flight case. (a) $r/R = 90\%$, (b) $r/R = 75\%$, (c) $r/R = 60\%$, $\mu = 0.186, \gamma = 6°$.

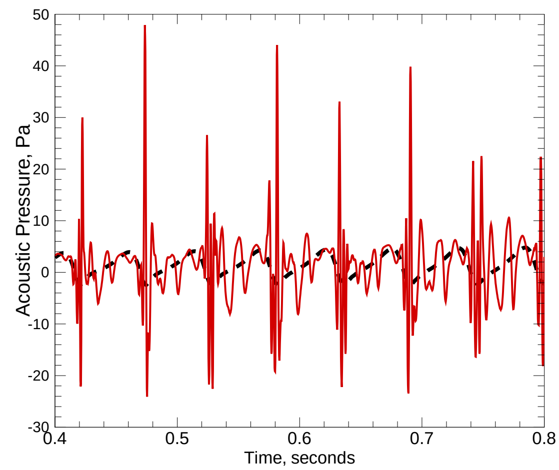


Figure 17: Acoustic pressure time history for the steady 6-degree descent at an observer location 3.73$R$ below, 4.59$R$ ahead, and 4.59$R$ on the advancing side of on the main rotor at $t = 0. \mu = 0.186, \gamma = 6°$. – – – GENHEL loading; ——— free-vortex wake model loading.

for the steady descent case, the acoustic pressure peaks are much higher when BVI is included in the simulation. At this observer position, the BVI noise peaks seem to generally increase and decrease as like the nonimpulsive component of the noise (i.e., the GENHEL loading result), but there are also significant BVI peaks in the time history near $t = 0.5$s and $t = 1.8$s. The acoustic pressure at these times actually has the maximum amplitude of the entire maneuver. It is unclear whether this result has physical or numerical significance, but these events occur near the initiation and cessation of the control inputs. A closer examination of the blade and vortex dynamics is needed to fully understand this result.

## Concluding Remarks

In the present study a free-vortex wake method was used to calculate the rotor wake and corresponding unsteady blade loads during several maneuvers. These loads were then used as input to PSU-WOPWOP to calculate the noise produced.

It was demonstrated that in moderate axial flight maneuvers most BVIs are perpendicular to the blade and are not important acoustically. In forward, descending flight, however, BVI noise is far more important. In an arrested descent maneuver the directivity and magnitude of the noise changes dramatically during the maneuver, and a simplified analysis will clearly miss the most significant features of the radiated noise and not adequately represent the overall noise directivity. The simplified blade loading model is only able to predict the character of the nonimpulsive component of acoustic pressure. An accurate vortex wake model is required to perform the aerodynamic calculations in these cases, and the free-vortex wake model provides a good balance of accuracy and computational complexity.

The results reported in this paper provide insight into the challenges that remain in the prediction of maneuver noise: the exact causes of the changes in directivity have yet to be identified, for example, and only a small subset of maneuvers has been analyzed. These issues and many others must be addressed in the future, but the present study provides a useful starting point for understanding low frequency and BVI noise.

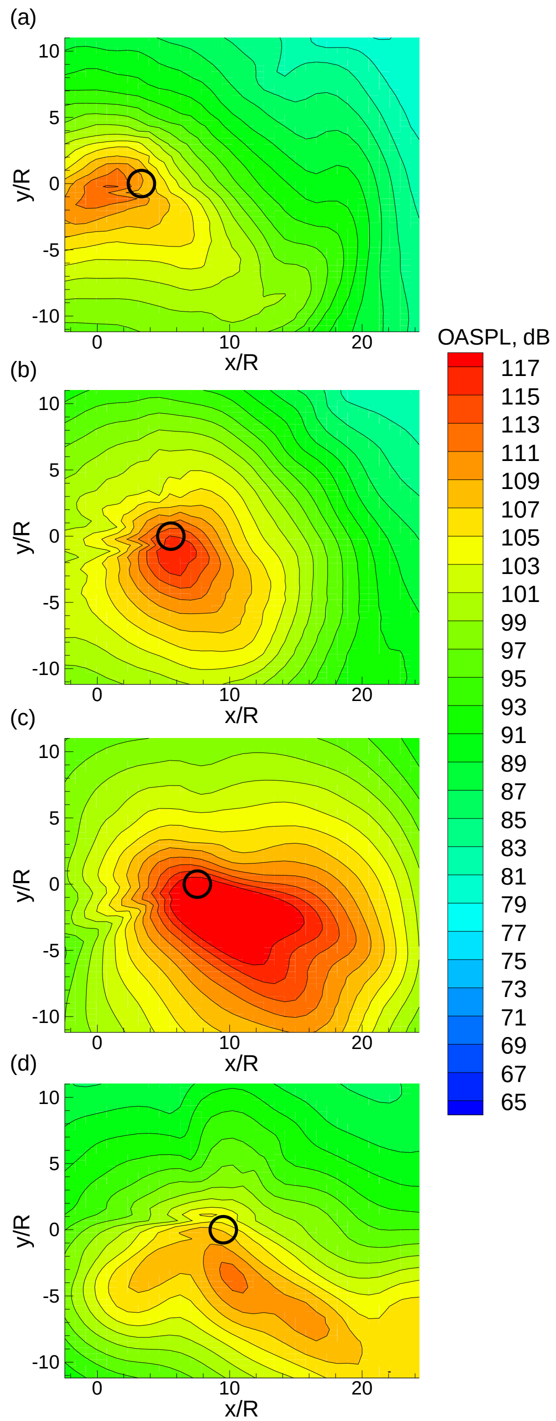


Figure 18: OASPL contours on a plane 3.73$R$ below the main rotor during the arrested descent maneuver. The rotor hub is at $x = 0$, $y = 0$ at time $t = 0$ and a Hanning window function with period 0.2s was used to in the Fourier analysis. The dark circle represent the projection of the main rotor onto the observer plane. The center of the Hanning window was at: (a)$t = 0.7$s; (b) $t = 1.1$s; (c)$t = 1.5$s; (d)$t = 1.9$s.

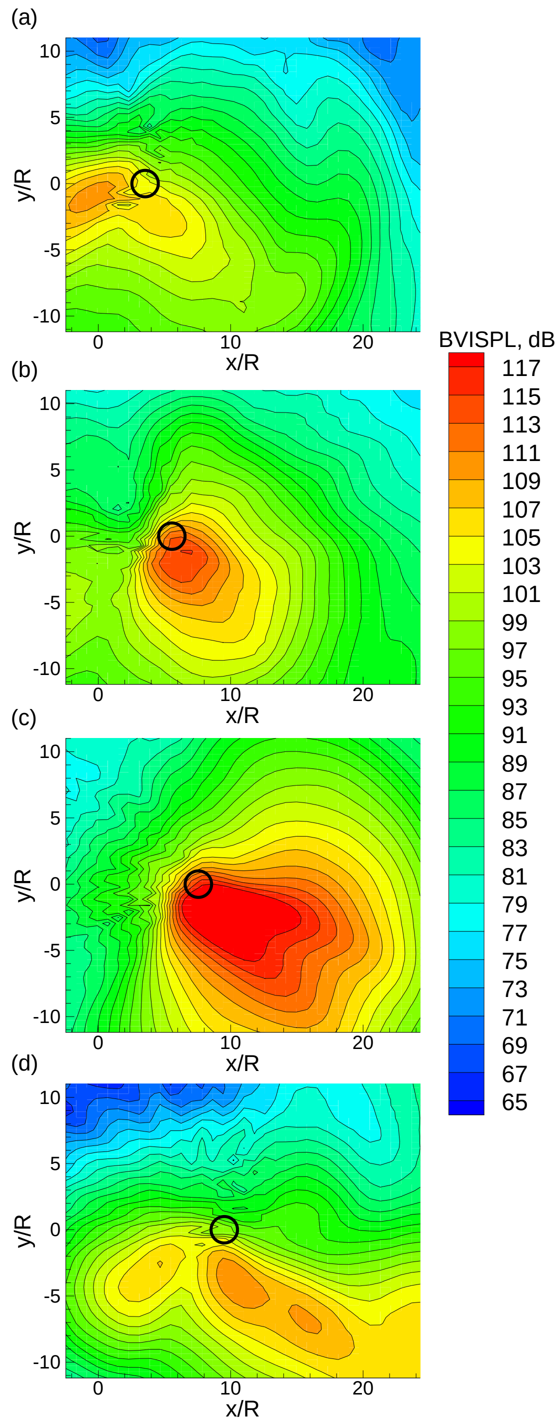


Figure 19: BVISPL (7th – 50th harmonics of blade passage period) contours on a plane 3.73$R$ below the main rotor during the arrested descent maneuver. The rotor hub is at $x = 0$, $y = 0$ at time $t = 0$ and a Hanning window function with period 0.2s was used to in the Fourier analysis. The dark circle represent the projection of the main rotor onto the observer plane. The center of the Hanning window was at: (a)$t = 0.7$s; (b) $t = 1.1$s; (c)$t = 1.5$s; (d)$t = 1.9$s.

## Acknowledgments

This work was supported by the National Rotorcraft Technology Center through the Rotorcraft Centers of Excellence Program under grants NCC 2994 and NGG 2-52275.

## References

1. Brentner, K. S., Brès, G. A., Perez, G., and Jones, H. E., "Maneuvering Rotorcraft Noise Prediction: A New Code for a New Problem," AHS Aerodynamics, Acoustics, and Test Evaluation Specialist Meeting, January 2002.

2. Brentner, K. S., Lopes, L. V., Chen, H. N., and Horn, J. F., "Near Real-Time Simulation of Rotorcraft Acoustics and Flight Dynamics," *Proceedings of American Helicopter Society 59th Annual Forum*, Phoenix, AZ, May 6-8 2003.

3. Howlett, J., "UH-60A BLACK HAWK Engineering Simulation Program: Volume I – Mathematical Model," Technical report, September 1989.

4. Bhagwat, M. J., and Leishman, J. G., "Stability, Consistency and Convergence of Time-Marching Free-Vortex Rotor Wake Algorithms," *Journal of the American Helicopter Society*, Vol. 46(1), January 2001, pp. 59–71.

5. Leishman, J. G., Bhagwat, M. J., and Bagai, A., "Free-Vortex Filament Methods for the Analysis of Helicopter Rotor Wakes," *Journal of Aircraft*, Vol. 39(5), Sept.-Oct. 2002, pp. 759–775.

6. Ananthan, S., and Leishman, J. G., "Predictions of Transient Wake Aerodynamics in Response to Time-Dependent Pilot Control Inputs," *Proceedings of the* 59*th* *Annual Forum of the American Helicopter Society International*, Pheonix, AZ, May 6–9 2003.

7. Carpenter, P. J., and Friedovich, B., "Effect of A Rapid Blade-Pitch Increase on the Thrust and Induced-Velocity Response of a Full-Scale Helicopter Rotor," Technical Report TN 3044, NACA, November 1953.

8. Jessurun, K. P., Pavel, M. D., and Toet, S., "Apparent Mass Effects on a Stiff-Hinged Rotor Model after Raid Cyclic and/or Collective Inputs - A Flow Visualization Study," 27*th* *European Rotorcraft Forum*, Moscow, Russia, Sept. 11-14 2001.

9. Leishman, J. G., Bhagwat, J. G., and Ananthan, S., "The Vortex Ring State as a Spatially and Temporally Developing Wake Instability," *American Helicopter Society International Aerodynamics Meeting*, San Fransisco, CA, Jan. 2002.

10. Gaonkar, G. H., and Peters, D. A., "Effectiveness of Current Dynamic Inflow Models in Hover and Forward Flight," *Journal of the American Helicopter Society*, Vol. 31(2), April 1986, pp. 47–57.

11. Rosen, A., and Isser, A., "A New Model for Rotor Dynamics During Pitch and Roll of a Hovering Helicopter," *Journal of the American Helicopter Society*, Vol. 40(3), 1995, pp. 17–28.

12. Keller, J. D., and Curtiss, H. C., "Modeling the Induced Velocity of a Maneuvering Helicopter," *American Helicopter Society 52nd Annual National Forum*, Washington, DC, June 4–6, 1996.

13. Barocela, E., Peters, D. A., Kothapalli, K. R., and Prasad, J. V. R., "The Effect of Wake Distortion on Rotor Inflow Gradients and Off-Axis Coupling," *AIAA Flight Mechanics Conference Proceedings*, San Diego, CA, July 29–31, 1997.

14. Bagai, A., Leishman, J. G., and Park, J., "Aerodynamic Analysis of a Helicopter in Steady Maneuvering Flight Using a Free-Vortex Rotor Wake Model," *Journal of the American Helicopter Society*, Vol. 44(2), April 1999, pp. 109–120.

15. Cottet, G.-H., and Koumoutsakos, P. D., *Vortex Methods: Theory and Practice*, Cambridge University Press, Cambridge, 2000.

16. Batchelor, G. K., *An Introduction to Fluid Dynamics*,, Cambridge University Press, Cambridge, UK, 1967, p. 87.

17. Ananthan, S., Leishman, J. G., and Ramasamy, M., "The Role of Filament Stretching in the Free-Vortex Modeling of Rotor Wakes," *American Helicopter Society 58*th *Annual Forum*, Montréal, Canada, June 11–13, 2002.

18. Johnson, W., *Helicopter Theory*,, Princeton University Press, 1980.

19. Weissinger, J., "The Lift Distribution of Swept-Back Wings," Technical Report TM 1120, NACA, 1947.

20. Leishman, J. G., "Aeroacoustics of 2-D and 3-D Blade Vortex Interaction Using the Indicial Method," *American Helicopter Society 52nd Annual Forum*, Washington, DC, June 4–6, 1996.

21. Leishman, J. G., "Subsonic Unsteady Aerodynamics Caused by Gusts Using the Indicial Method," *Journal of Aircraft*, Vol. 33(5), Sept.-Oct. 1996, pp. 869–879.

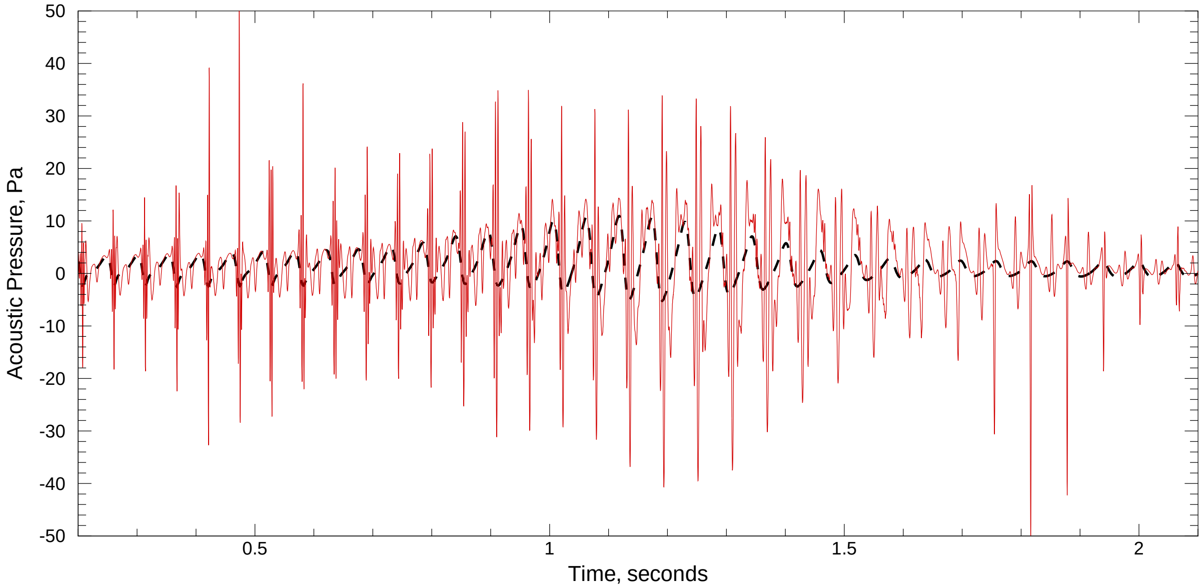


Figure 20: Acoustic pressure time history for the arrested descent maneuver at an observer location 3.73*R* below, 4.59*R* ahead, and 4.59*R* on the advancing side of on the main rotor at $t = 0$. – – – GENHEL loading; ——— free-vortex wake model loading.

22. Farassar, F., and Succi, G. P., "The Prediction of Helicopter Discrete Frequency Noise," *Vertica*, Vol. 7(4), 1983, pp. 309–320.

23. Brentner, K. S., and Farassat, F., "Analytical Comparison of the Acoustic Analogy and Kirchoff Formulation for Moving Surfaces," *AIAA Journal*, Vol. 36(8), August 1998, pp. 1379–1386.

24. Advanced Rotocraft Technology, I., "Kirchhoff Code – a Versatile CAA Tool," NASA SBIR Phase I Final Report, 1995. Contract NAS1-20366.

25. Leishman, J. G., "Aeroacoustics of 2D and 3D Blade-Vortex Interaction Using the Indicial Method," American Helicopter Society 52nd Annual Forum Proceedings, June 1996.

26. Bendat, J. S., and Piersol, A. G., *Engineering Applications of Correlation and Spectral Analysis*, John Wiley & Sons, Inc., New York, NY, 2nd edition, 1993.